

Laser-induced spin protection and switching in a specially designed magnetic dot: A theoretical investigation

G. P. ZHANG^{1 (a)}, M. S. SI¹ AND T.F. GEORGE²

¹ *Department of Physics, Indiana State University, Terre Haute, Indiana 47809, USA*

² *Office of the Chancellor and Center for Nanoscience, Departments of Chemistry & Biochemistry and Physics & Astronomy, University of Missouri-St. Louis, St. Louis, MO 63121 USA*

PACS 75.78.Jp –

PACS 75.50.-c –

PACS 78.47.jb –

Abstract – Most laser-induced femtosecond magnetism investigations are done in magnetic thin films. Nanostructured magnetic dots, with their reduced dimensionality, present new opportunities for spin manipulation. Here we predict that if a magnetic dot has a dipole-forbidden transition between the lowest occupied molecular orbital (LUMO) and the highest unoccupied molecular orbital (HOMO), but a dipole-allowed transition between LUMO+1 and HOMO, electromagnetically induced transparency can be used to prevent ultrafast laser-induced spin momentum reduction, or spin protection. This is realized through a strong dump pulse to funnel the population into LUMO+1. If the time delay between the pump and dump pulses is longer than 60 fs, a population inversion starts and spin switching is achieved. These predictions are detectable experimentally.

Introduction. – The discovery of femtosecond demagnetization in ferromagnetic Ni [1], which has attracted tremendous attention worldwide [2–7], challenges traditional wisdom and opens a new technological frontier for fast magnetic switching. The nonthermal inverse Faraday effect [8] is an excellent example, where one can manipulate the spin via the polarization of light, without involvement of the lattice. This has further inspired new theoretical and experimental investigations into the mechanism of the femtosecond magnetism. Up to now, while the experimental focus has been on thin films and bulk materials [9, 10], magnetic nanostructures, with reduced dimensionality, unique symmetry and quantum confinement, are very attractive. For instance, their electronic and magnetic properties can be tailored systematically. Experimental studies in cobalt nanostructures show very pronounced spin excitations [11]. This presents a unique opportunity for electromagnetically induced transparency (EIT) in a spin system. EIT has been demonstrated in atoms and molecules [12], and can be realized in some special designed quantum dots, with a proper state symmetry. EIT in a three-level system relies on two coherent laser pulses: one as a control pulse and the other as a

probe pulse. The absorption of the probe depends on the control pulse (see fig. 1). It would be fantastic if such EIT can be realized in a magnetic dot, since one can then fully integrate the light control into the magnetic storage on a femtosecond time scale, a daunting but technologically significant task. This motivates us to pursue such a system.

In this paper, we show that in a carefully designed magnetic dot, EIT can be used to protect spin momentum reduction. Using two laser pulses, one pump and one dump, we can not only protect a spin state but also switch it. The former is done through EIT, and the latter is achieved through population inversion. Spin protection does not occur naturally in any magnetic dots. The minimum condition for this to occur is that the optical transition between the lowest unoccupied molecular orbital (LUMO) and the highest occupied molecular orbital (HOMO) must be dipole-forbidden, while the transition between HOMO and LUMO+1 or higher states is dipole-allowed. The spin-orbit coupling must not be zero. Our investigation is based on two different theoretical formalisms. We start with the first-principles calculation in ferromagnetic fcc bulk nickel, and we then construct a model system with nearly identical electronic and magnetic properties. The model system allows us to search the best candidate for spin protection

(a)

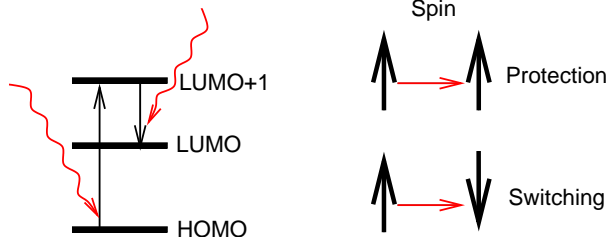


Fig. 1: Laser-induced spin protection and spin switching. A three-level system is shown. The transition between LUMO and HOMO is forbidden.

Table 1: Eigenvalues, and spin and orbital momenta of fcc Ni at k -point of $k = (101, 69, -7)/104$. All the results are computed using the first-principles method. The Fermi energy is at 0 eV. The k -mesh is $104 \times 104 \times 104$, so all the numbers are divided by 104.

i	\mathcal{E}_i (eV)	$S_z(\hbar)$	$L_z(\hbar)$
1	-4.065	0.499	-0.009
2	-3.740	0.496	-0.049
3	-3.691	-0.494	0.003
4	-3.112	-0.498	0.054
5	-2.311	0.496	-0.024
6	-1.682	-0.489	0.019
7	-1.109	0.490	0.052
8	-0.565	0.174	-0.028
9	-0.499	-0.174	-0.001
10	0.351	-0.499	-0.017
11	4.863	0.500	0.002
12	5.086	-0.500	-0.003
13	9.873	0.498	-0.008
14	10.040	-0.487	0.007
15	10.261	0.487	0.009
16	10.434	-0.498	-0.008
17	12.152	0.500	0.001
18	12.252	-0.500	-0.001

and switching. Future experiments can directly test our predictions.

This paper is arranged as follows. In the second section, we present our theoretical scheme, followed by the laser-induced ultrafast demagnetization in the third section. The spin protection and switching is presented in the fourth section, and we conclude this paper in the fifth section.

Theoretical formalism. – The first-principles method is certainly a method of choice for quantum dots, but there is a limit on what the method can do. It is difficult to isolate one physical quantity without affecting others in question. For instance, the spin-orbit coupling is a joint effect of the crystal potential and electron wavefunction, and can not be parametrized easily at the first-principles level. To strike a balance between a real system

Table 2: Eigenvalues (\mathcal{E}_i) and their spin (S_z) and orbital momenta (L_z). The spin-orbit coupling is chosen as $\lambda = 0.05$ eV. The Fermi energy is set between d_5 and d_6 in order to have small orbital and large spin momenta.

i	Orbital type	\mathcal{E}_i (eV)	$S_z(\hbar)$	$L_z(\hbar)$
1	d_1	-2.496	0.444	-0.072
2	d_2	-2.271	-0.443	0.073
3	d_3	-1.754	0.479	0.008
4	d_4	-1.547	-0.479	-0.009
5	d_5	-0.750	0.497	-0.003
6	d_6	-0.550	-0.497	0.003
7	p_1	0.015	0.350	-0.013
8	p_2	0.086	-0.350	0.013
9	d_7	0.248	0.487	-0.016
10	d_8	0.452	-0.486	0.017
11	d_9	0.973	0.448	0.068
12	d_{10}	1.195	-0.450	-0.069
13	p_3	1.440	0.499	-0.001
14	p_4	1.490	-0.499	0.001
15	p_5	2.845	0.357	0.012
16	p_6	2.915	-0.357	-0.012

and a model system, we first perform a first-principles investigation in fcc nickel. While details have been presented elsewhere [13], here in brief we use the full-potential augmented plane wave method within the density functional formalism as implemented in the WIEN2k code [14]. By solving the Kohn-Sham equation (in Ry atomic units),

$$[-\nabla^2 + V_{Ne} + V_{ee} + V_{xc}^\sigma] \psi_{i\mathbf{k}}^\sigma(r) = E_{i\mathbf{k}}^\sigma \psi_{i\mathbf{k}}^\sigma(r), \quad (1)$$

we obtain the eigenfunctions and eigenenergies, from which we construct the spin and orbital matrix elements among all the band states. In eq. (1), the first and second terms are kinetic energy and Coulomb interaction between the electron and the nuclei, and V_{xc} is the Coulomb and exchange interactions. The spin-orbit coupling is included via the second-order variational method. In table 1, we show the eigenenergies, spin and orbital matrix elements at one crystal momentum point k . These elements are the basis for our model.

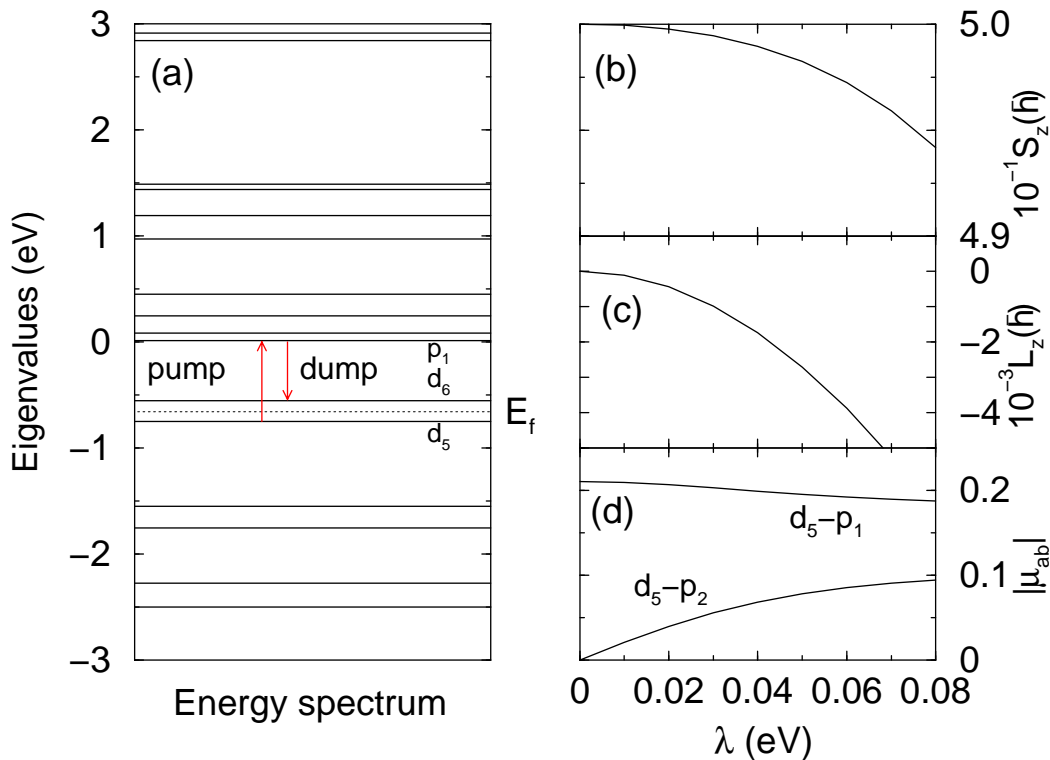


Fig. 2: (a) Energy spectrum. The results are obtained with $\lambda = 0.05$ eV. E_f represents the Fermi energy. The pump laser is tuned to the transition between d_5 and p_1 , while the dump to the transition between d_6 and p_1 . (b) Ground-state spin angular momentum change as a function of λ . (c) Ground-state orbital angular momentum change with λ . (d) Transition matrix elements $|\mu_{ab}|$ between d_5 and p_1 and between d_5 and p_2 as a function of λ .

We introduce a sixteen-level model, with the spin-orbit coupling as an input parameter. The model consists of three p -orbitals (Y_{11} , Y_{10} and Y_{1-1}) and five d -orbitals (Y_{22} , Y_{21} , Y_{20} , Y_{2-1} , and Y_{2-2}) for each spin channel. Here the Y_{lm} 's are the spherical harmonics, and the radial part of the wavefunction is included through the parameters (see below). The overlap between p - and d -orbitals is ignored to minimize the number of parameters used, but the overlap between d -orbitals and that between p -orbitals are introduced. To mimic a ferromagnetic ground state, these d -orbitals lie about 2 eV below the p -orbitals. Within these approximations, our Hamiltonian consists of two parts, $H_0 = H_d + H_p$. Here the Hamiltonian for d -states is

See eq. 2

where $\varepsilon_{d\sigma}$ is the d -orbital energy with spin index σ , \vec{l} is the orbital angular momentum operator, and \vec{s} is the spin angular momentum operator. $c_{m\sigma}^\dagger$ ($c_{m\sigma}$) is the electron creation (annihilation) operator, creating (annihilating) an electron in orbital m . We choose the spin-orbit coupling (SOC) constant $\lambda = 0.05$ eV, except in figs. 2(b), 2(c) and 2(d). The Dirac bracket $|2, m, \sigma\rangle$ in eq. (2) represents Y_{2m} multiplied by the spin wavefunction $|\sigma\rangle$. The last term, originating from the crystal and exchange fields, de-

notes the overlap between orbitals with different m , with $\delta = 1$ eV. (A similar Hamiltonian can be set up for the p -orbitals.) Based on our first-principles calculation for fcc Ni [9, 13], we choose $\varepsilon_{d\uparrow} = -0.75$ eV, $\varepsilon_{d\downarrow} = -0.55$ eV, $\varepsilon_{p\uparrow} = 1.44$ eV and $\varepsilon_{p\downarrow} = 1.49$ eV. While the precise orbital energies are not critical here, in order to realize a strong spin momentum, we find it is necessary to adjust the overlap term if different orbital energies are used. An extension to f -orbitals is straightforward.

We first compute the spin, orbital and dipole transition matrices by diagonalizing the Hamiltonian. The orbital characters of the eigenstates are determined by their eigenvectors. The eigenvalues, spin and orbital momenta are tabulated in table 2. The six lowest eigenstates are all d -states, followed by two p -states. It is clear from the table that to realize large spin but small orbital momenta, the number of occupied states is not arbitrary. We choose the Fermi energy between d_5 and d_6 so the five lowest d -orbitals are occupied. The resultant ground-state spin momentum is $\langle s_z \rangle = 0.498\hbar$, and the orbital momentum is $\langle l_z \rangle = -0.0027\hbar$. This result can be compared with our first-principles results in table 1, and we find that they match very well. For instance, the majority of spin values are around $0.5\hbar$ and the orbital momentum is below $0.1\hbar$. This gives us confidence that our model is able to simulate

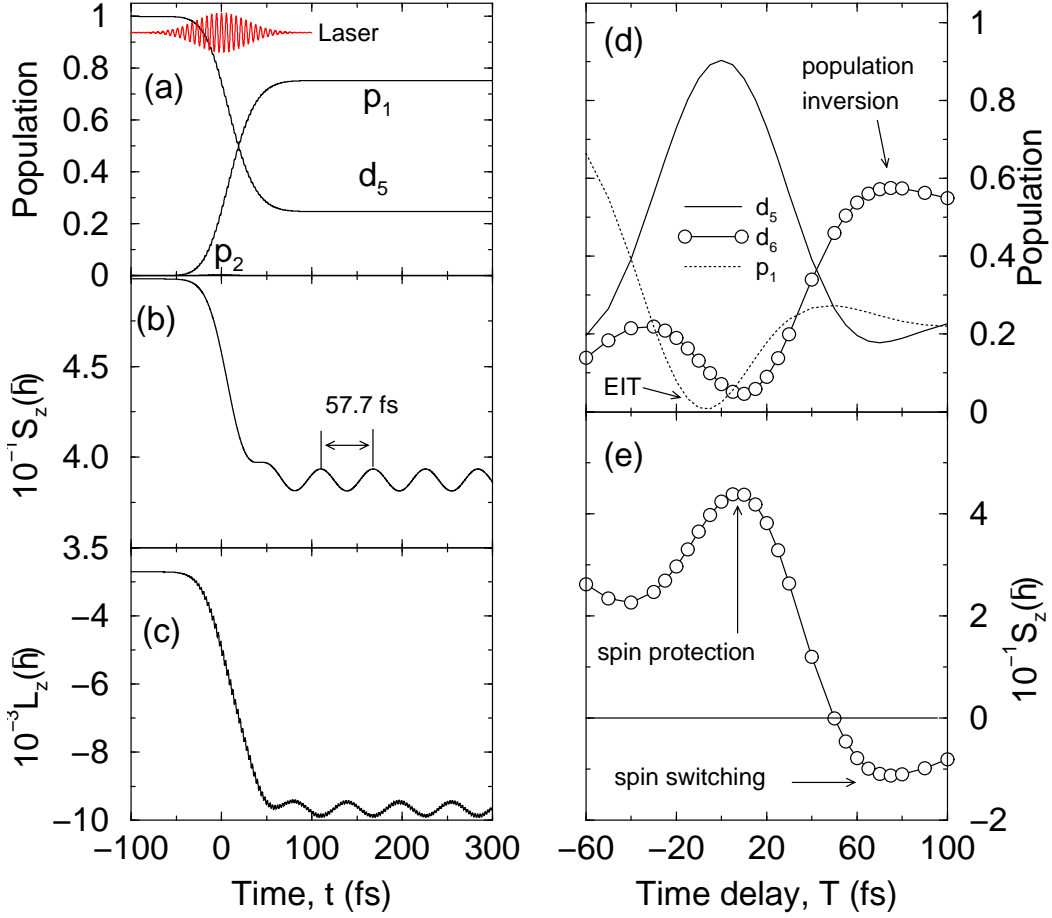


Fig. 3: (a) Population change as a function of time upon laser excitation. Only the three states p_1 , p_2 and d_5 are shown (the population in all the other states is nearly unchanged). Inset: Laser pulse. (b) Spin momentum change as function of time. The oscillation is due to the interference between states p_1 and p_2 . (c) Orbital angular momentum change. (d) Population change excited by pump and dump pulses as a function of the time delay between the two pulses. Electromagnetically induced transparency (EIT) occurs for the transition between d_5 and p_1 when the delay is close to 0 fs, and population inversion occurs for the delay longer than 60 fs. (e) Change from spin protection to spin switching, where the time delay between the pump and dump pulses is longer than 60 fs.

a ferromagnetic system.

Figure 2(a) shows the energy spectrum with the relevant transition states labeled. Figures 2(b) and 2(c) show the dependence of the spin (s_z) and orbital angular momenta (l_z) on the SOC constant λ . It is interesting to note that the spin decreases with λ , but we also find this to be parameter dependent, and in some cases the dependence is not monotonic. The orbital momentum is zero if λ is zero, or complete quenching, but with nonzero λ the quenching is not complete. This reproduces the well-known fact that the SOC drags some orbital momentum with it. We find transition matrix elements are larger between two states with a similar spin moment, which independently validates our prior first-principles results [13, 15]. For instance, the transition matrix element (z -direction) between d_5 ($s_z = 0.497\hbar$) and p_1 ($s_z = 0.350\hbar$) is 0.196ξ , while the element between d_5 ($s_z = 0.497\hbar$) and p_2 ($s_z = -0.350\hbar$) is -0.078ξ , where ξ is a constant

resulting from the radial part of the wavefunction. This demonstrates again that our model is applicable to ferromagnetic systems. Therefore, even with SOC, the optical transition still prefers spin-conserved transitions over spin-nonconserved transitions, though for the demagnetization process, the latter transitions are most important. The systematic change of the transition matrix elements with the SOC for the above two transitions is shown in fig. 2(d). To our knowledge, this is the first numerical result that shows clearly the transition matrix element drops for a “spin-conservation” transition (here between d_5 and p_1), while the elements for the spin-flip transition (between d_5 and p_1) increase. This demonstrates the critical role of the SOC in ultrafast demagnetization.

Laser-induced coherent magnetization. – To simulate the ultrafast spin evolution, we introduce a laser pulse with $E_i(t) = A_i \cos(\omega_i t) \exp[-(t - t_i)^2 / \tau_i^2]$, where A_i , ω_i , t_i and τ_i are the laser amplitude, frequency, time

$$H_d = \sum_{m\sigma} \varepsilon_{d\sigma} c_{m\sigma}^\dagger c_{m\sigma} + \sum_{m_1, m_2; \sigma_1, \sigma_2} \lambda \langle 2, m_1, \sigma_1 | \vec{l} \cdot \vec{s} | 2, m_2, \sigma_2 \rangle c_{m_1 \sigma_1}^\dagger c_{m_2 \sigma_2} + \sum_{m\sigma} \delta c_{m+1\sigma}^\dagger c_{m\sigma} + h.c. , \quad (2)$$

delay and pulse duration of pulse i , respectively, and t is time. The laser has a Gaussian shape, with duration of 40 fs (see the inset of fig. 3(a)). We tune the laser frequency to be resonant with the dipole-allowed transition between d_5 and p_1 . The dynamic simulation starts with solving the Liouville equation for the density matrix ρ as [4, 13, 16],

$$i\hbar \frac{\partial \rho}{\partial t} = [H, \rho], \quad (3)$$

where H consists of the Hamiltonians H_d and H_p for the d - and p -states and the interaction H_I between the system and laser field. $H_I = -eE(t) \sum_{ij} \langle i|z|j \rangle c_i^\dagger c_j$, where $-e$ is the electron charge, the light polarization is along the z -direction, and $\langle i|z|j \rangle$ is the transition matrix element between states i and j . The merit of our approach should not be underestimated. Although the Liouville equation is equivalent to the time-dependent Schrödinger equation, the Liouville equation naturally takes into account the Pauli exclusion principle and includes the antisymmetry of the many-body wavefunction. However, most of the time-dependent Schrödinger equations from textbooks are for a single particle only, which is not suitable even for a non-interacting case.

The general form of the density matrix is a convoluted integration equation. We express the density matrix in a state representation as

$$i\hbar \frac{\partial \rho_{nm}}{\partial t} = (\mathcal{E}_n - \mathcal{E}_m) \rho_{nm} + \sum_k (H_{nk}^I \rho_{km} - \rho_{nk} H_{km}^I), \quad (4)$$

where k , n and m are the state indices, \mathcal{E}_n is the eigenenergy of state n , ρ_{nm} is the density matrix between states n and m , and H^I is the interaction between the laser field and the system. If we integrate over time, we have

See eq. 5

which is the general form of the density matrix. It is clear that the time evolution of the density depends on its history and the laser field. Further simplifications are possible, only if we know the profile of the laser field. For instance, if the laser is a continuous wave and is very weak, the density matrix can be approximated by the first order density matrix whose time evolution is proportional to $\exp[-i(\omega_{laser} - \omega_{nm})t]$, where ω_{nm} is the transition frequency between states n and m , ω_{laser} is the laser frequency, and t is the time. If the laser is a pulse, then the profile of the density matrix sensitively depends on the laser pulse duration, laser frequency and the electronic states involved as can be seen from the above equation. In this case, an analytic solution is generally not possible, and a numerical integration is a must.

Figure 3(a) shows that the population change closely follows the profile of the laser field. Upon the laser excitation, the d_5 -state loses its population from 1 to 0.25 within the first 40 fs. In the meantime, the p_1 -state gains the same amount of population from 0 to 0.75. Other states have a very small change. For instance, p_2 only has a tiny increase around 0 fs. Once the laser field is over, the population or diagonal element of the density matrix ρ_{ii} change is stabilized. However, this does not mean that all the elements of the density matrix become time independent. The interference between states, which is induced by the laser field initially, remains. This is precisely what happens with the spin momentum change.

Figure 3(b) shows the spin change as a function of time. The spin drops similarly within the first 40 fs, followed by an oscillation with period 57.7 fs. The first drop results from the spin momentum difference between d_5 and p_1 , as seen from table 2, where $\langle d_5 | s_z | d_5 \rangle = 0.497\hbar$ and $\langle p_1 | s_z | p_1 \rangle = 0.350\hbar$. The oscillation is from the interference between p_1 and p_2 , which can be verified by switching on/off the density matrix element ρ_{p_1, p_2} . It is remarkable that even though the population of p_2 is almost zero, its interference with p_1 is directly responsible for this salient change. The period 57.7 fs corresponds to 0.071 eV, which matches the energy gap between p_1 and p_2 exactly. The orbital momentum change is shown in fig. 3(c). In contrast to the spin change, the orbital angular momentum increases (more negative). Besides its initial drop, the orbital momentum also has smaller rapid beatings.

Spin protection and switching. – As mentioned in the Introduction, the key to the electromagnetically induced transparency relies on the state symmetry. In the following, we demonstrate that one can not only reduce and flip a spin (spin switching), but also protect it (spin protection). We employ two laser pulses, one pump with field $E_1(t)$ and one dump with $E_2(t)$ [17]. The laser parameters of the pump are the same as above. The dump is tuned to the transition between p_1 and d_6 (see fig. 2(a)), with duration of 60 fs and field amplitude of 2.5 times the pump. These parameters are carefully chosen to maximize the effect and are fixed below. The only variable is the time delay $T = t_1 - t_2$ between the pump and dump. Figure 3(d) shows the populations as a function of T for three states, with the solid line for the originally occupied d_5 -state, dashed line for the originally unoccupied p_1 -state, and circle line for the originally unoccupied d_6 -state. Negative time delay means the dump proceeds earlier than the pump. The results in figs. 3(d) and 3(e) are computed after $t = 200$ fs. If the results oscillate with time, we show the time-averaged data. At $T = -60$ fs, similar to the above single-pump-pulse excitation, d_5 loses population to p_1 , but now the d_6 -state gains some popu-

$$\rho_{nm}(t) = \frac{1}{i\hbar} \int_{-\infty}^t dt' (\mathcal{E}_n - \mathcal{E}_m) \rho_{nm}(t') + \frac{1}{i\hbar} \sum_k \int_{-\infty}^t dt' (H_{nk}^I(t') \rho_{km}(t) - \rho_{nk}(t') H_{km}^I(t')), \quad (5)$$

lation, in sharp contrast to the above single-pulse excitation. When T decreases (less negative), the population in d_5 increases sharply, but the populations in p_1 and d_6 drop sharply. In other words, the system becomes more difficult to excite and much less absorptive, or transparent to the light field. This is a manifestation of electromagnetically induced transparency (EIT) [18], though in EIT normally cw lasers are used [18]. What is novel here is that a time delay can induce EIT, which has a direct consequence in the spin change. Figure 3(e) illustrates that during EIT, the spin is mostly unchanged, i.e., spin protection. What is even more interesting is that when we increase the time delay over 60 fs, population inversion starts.

Going back to fig. 3(d), we see that the population in d_6 becomes largest and that in d_5 drops below both d_6 and p_1 , a total population inversion. Now if we monitor the spin change at the same delay, we find that s_z changes its sign from positive to negative (see fig. 3(e)), or spin switching. We expect our predictions are detectable experimentally in magnetic systems whose electronic and magnetic structures are similar to those of our model. The key to the successful realization of EIT is that the dipole-transition between the LUMO and HOMO must be forbidden and the transition between HOMO and LUMO+1 or higher states is allowed. Very recently, Hübner *et al.* demonstrated the optical spin manipulation for magnetic logic operations in the Ni_3Na_2 cluster [19, 20]. Therefore, the possibility to observe our prediction is very high.

Conclusions. – We have demonstrated a new electromagnetically induced spin protection and switching in a specially designed magnetic dot. The minimum requirement for such a dot is that the optical transition is allowed between the HOMO and LUMO+1, but not HOMO and LUMO. A strong dump pulse couples LUMO and LUMO+1, and directly controls the spin dynamics. As a result, the spin becomes harder to excite, i.e., spin protection. We have also shown that if the time delay between the pump and dump laser pulses exceeds 60 fs, a spin switch from spin up to spin down occurs. We expect both these predictions are detectable experimentally.

This work was supported by the U. S. Department of Energy under Contract No. DE-FG02-06ER46304. We acknowledge part of the work as done on Indiana State University's high-performance computers, which is supported by the Center for Instruction, Research and Teaching. This research used resources of the National Energy Research Scientific Computing Center at Lawrence Berkeley National Laboratory, which is supported by the Office of Science of the U.S. Department of Energy under Contract No. DE-AC02-05CH11231. Initial studies used resources of the Argonne Leadership Computing Facility at

Argonne National Laboratory, which is supported by the Office of Science of the U.S. Department of Energy under Contract No. DE-AC02-06CH11357.

*Electronic address: gpzhang@indstate.edu

REFERENCES

- [1] BEAUREPAIRE E., MERLE J.-C., DAUNOIS A. and BIGOT J.-Y. *Phys. Rev. Lett.*, **76** (1996) 4250.
- [2] BOEGLIN C. *et al.*, *Nature*, **465** (2010) 458; KOOPMANS B. *et al.*, *Phys. Rev. Lett.*, **95** (2005) 267207.
- [3] KOOPMANS B. *et al.*, *Nature Mater.*, **9** (2010) 259 (2010); MÜNZENBERG M. G., *Nature Mater.*, **9** (2010) 184; ATXITIA U., *Phys. Rev. B*, **81** (2010) 174401.
- [4] ZHANG G. P., HÜBNER W., LEFKIDIS G., BAI Y. and GEORGE T. F., *Nature Phys.*, **5** (2009) 499.
- [5] BIGOT J.-Y., VOMIR M. and BEAUREPAIRE E., *Nature Phys.* **5** (2009) 515.
- [6] LEFKIDIS G., ZHANG G. P. and HÜBNER W., *Phys. Rev. Lett.*, **103** (2009) 217401.
- [7] SI M. S. and ZHANG G. P., *J. Phys.: Condens. Matter*, **22** (2010) 076005.
- [8] STANCIU C. D. *et al.*, *Phys. Rev. Lett.*, **99** (2007) 047601.
- [9] ZHANG G. P. and HÜBNER W., *Phys. Rev. Lett.*, **85** (2000) 3025.
- [10] MALIK D. A. *et al.*, *Phys. Rev. Lett.*, **104** (2010) 133001.
- [11] VARALDA J. *et al.*, *Phys. Rev. B*, **83** (2011) 045205; DEMPSEY K. J. *et al.*, *Phys. Rev. B*, **82** (2010) 214415; SMIRNOV A. A. and PANKRATOV A. L., *Phys. Rev. B*, **82** (2010) 132405; DEY S. *et al.*, *Chem. Phys. Lett.*, **492** (2010) 281; MASSA L. *et al.*, *J. Superconductivity & Novel Magnetism*, **23** (2010) 121; BIGOT J.-Y. *et al.*, *Chem. Phys.*, **318** (2005) 137.
- [12] FLEISCHHAUER M., IMAMOGLU A. and MARANGOS J. P., *Rev. Mod. Phys.*, **77** (2005) 633.
- [13] ZHANG G. P., BAI Y. and GEORGE T. F., *Phys. Rev. B*, **80** (2009) 214415.
- [14] BLAHA P. *et al.*, WIEN2k, An Augmented Plane Wave + Local Orbitals Program for Calculating Crystal Properties (Techn. Universität Wien, Austria, 2001).
- [15] ZHANG G. P. and GEORGE T. F., *Phys. Rev. B*, **78** (2008) 052407.
- [16] ZHANG G. P., *Phys. Rev. Lett.* **101** (2008) 187203.
- [17] OHTSUKI Y., YAHATA Y., KONO H. and FUJIMURA Y., *Chem. Phys. Lett.*, **287** (1998) 627.
- [18] HARRIS S. E., FIELD J. E. and IMAMOGLU A., *Phys. Rev. Lett.*, **64** (1990) 1107; BOLLER K.-J., IMAMOGLU A. and HARRIS S. E., *Phys. Rev. Lett.*, **66** (1991) 2593 (1991).
- [19] HÜBNER W., KERSTEN S. and LEFKIDIS G., *Phys. Rev. B*, **79** (2009) 184431.
- [20] LEFKIDIS G. and HÜBNER W., *Phys. Rev. Lett.*, **95** (2005) 077401 (2005); LEFKIDIS G. and Hübner W. *Phys. Rev. B*, **74** (2006) 155106; LEFKIDIS G. and HÜBNER W., *Phys. Rev. B*, **76** (2007) 014418.